Available online at www.sciencedirect.com
SCIENCE DIRECT®
International Journal of Heat and Mass Transfer 49 (2006) 3670–3680
International Journal of HEAT and MASS TRANSFER
www.elsevier.com/locate/ijhmt

Turbulent separated convection flow adjacent to backward-facing step—effects of step height

Y.T. Chen [a,*], J.H. Nie [a], B.F. Armaly [b], H.T. Hsieh [a]

[a] Department of Mechanical Engineering, University of Nevada, Las Vegas, Las Vegas, NV 89154, USA
[b] Department of Aerospace and Mechanical Engineering, and Engineering Mechanics, University of Missouri—Rolla, Rolla, MO 65409, USA

Received 8 November 2005; received in revised form 10 February 2006
Available online 27 April 2006

Abstract

Simulations of turbulent convection flow adjacent to a two-dimensional backward-facing step are presented to explore the effects of step height on turbulent separated flow and heat transfer. Reynolds number and duct's height downstream from the step are kept constant at $Re_0 = 28{,}000$ and $H = 0.19$ m, respectively. Uniform and constant heat flux of $q_w = 270$ W/m^2 is specified at the stepped wall downstream from the step, while other walls are treated as adiabatic. The selection of the values for these parameters is motivated by the fact that measurements are available for this geometry and they can be used to validate the flow and heat transfer simulation code. Two-equation low-Reynolds-number model is employed to achieve the turbulent Prandtl number. The primary and secondary recirculation regions increase in size as the step height increases. The bulk temperature increases more rapidly as the step height increases. Increasing the step height causes the magnitude of the maximum turbulent kinetic energy to increase. Near the step and below the step height, the turbulent kinetic energy becomes smaller as the step height increases. Inside the recirculation region, magnitude of the peak friction coefficient does not significantly change with the increase of step height. The friction coefficient becomes smaller in magnitude with the increase of the step height. The peak Stanton number becomes smaller as the step height increases.

1. Introduction

Flow separation and subsequent reattachment that are caused by sudden expansion in flow geometry occur in critical components of many practical applications where heating or cooling is required. These applications appear in gas turbine engines, electronic cooling equipment, combustors, as well as in external flows, including flows around buildings and aircraft, and many other heat transfer devices. This flow separation and reattachment almost always determines the key structure of the flow field and significantly influences the mechanism of heat transfer. A great deal of mixing of high and low energy fluid occurs in the separated and reattached flow regions, thus influencing significantly the performance of these devices. Studies on separated/reattached flow have been conducted extensively during the past decades, and the backward-facing step geometry received most of the attention (see, for example [1–3], and the references cited therein). This geometry is very simple, yet the flow and the heat transfer through it contain most of the features encountered in more complex geometries, and for that reason it has been used in benchmark studies [4–6] to validate simulation codes and algorithms.

The majority of published work on separated-reattached flow in this geometry deals with laminar flow. Effects of Reynolds number [3,7,8], step height [9,10], aspect ratio [11], and Prandtl number [7] were reported, which brought to light some of the flow and heat transfer features that develop in the laminar flow regime. However, comparatively little is published on the turbulent flow case. Such knowledge is needed for simulating and optimizing the performance of physical heat exchanging devices that are mostly working within turbulent flow regime. In addition, most of the published turbulent results in this geometry

* Corresponding author. Tel.: +1 7028951202; fax: +1 7028953936.
E-mail address: uuchen@nscee.edu (Y.T. Chen).

0017-9310/$ - see front matter © 2006 Elsevier Ltd. All rights reserved.
doi:10.1016/j.ijheatmasstransfer.2006.02.024

Nomenclature

A_{D1}, A_{D2}, C_λ, C_m constants in heat transfer model functions
C_f skin friction coefficient $= 2\tau_w/\rho u_0^2$
C_p specific heat
C_{P1}, C_{P2}, C_{D1}, C_{D2} constants in transport equation for ε_t
C_μ, $C_{\varepsilon 1}$, $C_{\varepsilon 2}$ constants in velocity field turbulence model
ER expansion ratio $= H/h$
f_μ, f_d, f_ε functions in velocity field turbulence model
f_{P1}, f_{P2}, f_{D1}, f_{D2} functions in temperature field turbulence model
H channel's height downstream of the step
h channel's height upstream of the step
I turbulence intensity
k turbulent kinetic energy $= \overline{u_i' u_i'}/2$
n normal direction to the wall surface
p mean static pressure
Pr, Pr_t molecular and turbulent Prandtl number
Re_0 Reynolds number based on channel centerline velocity $= u_0 S/\nu$
Re_m Reynolds number based on channel bulk velocity $= 2u_m\delta/\nu$
Re_τ Reynolds number based on friction velocity $= u_\tau\delta/\nu$
R_t turbulent Reynolds number $= k^2/\nu\varepsilon$
S channel's reference height
s step height
St Stanton number $= \frac{q_w}{\rho C_p u_0 (T_w - T_0)}$
T, t mean temperature and temperature fluctuation
T^+ non-dimensional mean temperature $= (T_w - T)/t_\tau$
T_0 inlet temperature
T_w wall temperature
t_τ friction temperature $= q_w H/(\rho C_p u_\tau)$
u, v velocity component in the x- and y-directions, respectively
u' velocity fluctuation
u^+ non-dimensional mean velocity $= u/u_\tau$
u_0 inlet freestream velocity upstream of the step
u_i general notation for mean velocity components ($u_1 = u$ and $u_2 = v$)
u_m bulk velocity
u_ε Kolmogorov velocity scale $= (\nu\varepsilon)^{1/4}$
u_τ friction velocity $= \sqrt{\tau_w/\rho}$
x, y streamwise and transverse coordinates, respectively
x_i general notation for coordinate directions ($x_1 = x$ and $x_2 = y$)
x_R flow reattachment length
y^+ non-dimensional distance from the wall surface $= u_\tau y/\nu$
y^* non-dimensional distance from the wall surface $= u_\varepsilon y/\nu$
y_n normal distance to the wall surface

Greek symbols
α, α_t molecular and eddy diffusivities for heat
δ 99% boundary layer thickness
δ_{ij} Kronecker delta
ε dissipation rate of turbulent kinetic energy $= \nu\overline{(\partial u_i'/\partial x_j)(\partial u_i'/\partial x_j)}$
ε_t dissipation rate of $\overline{t^2}/2 = \alpha\overline{(\partial t/\partial x_j)(\partial t/\partial x_j)}$
κ von Karman's universal constant
ρ density
ν, ν_t molecular kinematic and eddy viscosities
σ_k, σ_ε, σ_h, σ_φ model constants for turbulent diffusion of k, ε, $\overline{t^2}$ and ε_t
τ time
τ_w wall shear stress

focused on the fluid mechanics or isothermal case, and these include the experimental results using laser Doppler velocimetry (LDV) [12,13], particle image velocimetry (PIV) [14], particle-tracking velocimetry [15], hot-wire anemometry [16], and numerical simulations [17,18]. The surveys by Simpson [1] and Eaton and Johnson [2] highlight some of the available fluid mechanics studies. Sudden-expansion particle-laden flows were numerically investigated by Zhang et al. [19] using an improved stochastic separated flow model. Studies of turbulent separated flow and heat transfer have been limited to only a few specific studies [20–22]. The enhancement of heat transfer in turbulent separated and reattaching flow over a backward-facing step by local forcing was simulated by Rhee and Sung [23] for different forcing frequencies. Since the constant turbulent Prandtl number cannot adequately predict the convection heat transfer around the separated and reattaching region, a diffusivity tensor heat transfer model was employed [23]. To the authors' knowledge, effects of step height in backward-facing step geometry (flow and heat transfer) have not appeared in the literature, and the lack of such results motivated the current study.

2. Method descriptions

Turbulence modeling in near-wall regions plays a crucial role in making accurate predictions, since turbulence structure is greatly influenced by the presence of a complex wall boundary. Several fundamental studies of turbulent separated and reattached flow exist in the literature including the results by Le et al. [17] using direct numerical simulation (DNS). Nevertheless, limitations on computational

power and memory make it almost impossible to directly solve the turbulent flow field in practical engineering flows using direct numerical simulation for the foreseeable future. Large eddy simulations (LES) may be more tractable; although to date, their use has not been widespread. Thus, the prediction of the turbulent flow and heat transfer characteristics in engineering equipment still requires a Reynolds-averaged approach using suitable turbulent closure models for both the velocity and temperature correlations [24].

Laws of the wall boundary conditions do not formally apply to complex turbulent flows with separation and reattachment. The standard two-equation k–ε model performs poorly for flows with strong separation, large streamline curvature, and adverse pressure gradient [25]. For complex flows with multiple wall surfaces, direct integration of turbulence equations on a solid boundary is required. In order to calculate turbulence quantities accurately in the near-wall region, a number of low-Reynolds-number versions of the turbulence model have been proposed [26–29]. These models are usually extended from high-Reynolds-number versions of the model by introducing various wall damping functions that are expressed in terms of the turbulent Reynolds number and the normal wall distance. The low-Reynolds number model proposed by Abe et al. [28,29] is selected for this study because the damping functions of this model introduce the Kolmogorov velocity (u_ε) instead of friction velocity (u_τ) as the velocity scale. This can avoid the singularity problems associated with the friction velocity at the separating and reattaching points. In addition, turbulent Prandtl numbers are achieved by solving the two-equation low-Reynolds-number model to mimic the variations in the turbulent Prandtl number around the reattachment region.

Two-dimensional turbulent forced convection flow adjacent to a backward-facing step is simulated. The Reynolds-averaged Navier–Stokes equation, the equations of the turbulent kinetic energy k for the velocity field and its dissipation rate ε, the energy equation, and the equations of the turbulent kinetic energy k_t for the thermal field and its dissipation rate ε_t are solved numerically together with the continuity equation using the finite volume method.

Continuity:

$$\frac{\partial u_i}{\partial x_i} = 0 \tag{1}$$

Two-equation model for velocity field:

$$\frac{\mathrm{D}u_i}{\mathrm{D}\tau} = -\frac{1}{\rho}\frac{\partial p}{\partial x_i} + \frac{\partial}{\partial x_j}\left\{ v\left(\frac{\partial u_i}{\partial x_j} + \frac{\partial u_j}{\partial x_i}\right) - \overline{u_i' u_j'} \right\} \tag{2}$$

$$\frac{\mathrm{D}k}{\mathrm{D}\tau} = \frac{\partial}{\partial x_j}\left\{ \left(v + \frac{v_t}{\sigma_k}\right)\frac{\partial k}{\partial x_j} \right\} - \overline{u_i' u_j'}\frac{\partial u_i}{\partial x_j} - \varepsilon \tag{3}$$

$$\frac{\mathrm{D}\varepsilon}{\mathrm{D}\tau} = \frac{\partial}{\partial x_j}\left\{ \left(v + \frac{v_t}{\sigma_\varepsilon}\right)\frac{\partial \varepsilon}{\partial x_j} \right\} - C_{\varepsilon 1}\frac{\varepsilon}{k}\overline{u_i' u_j'}\frac{\partial u_i}{\partial x_j} - C_{\varepsilon 2} f_\varepsilon \frac{\varepsilon^2}{k} \tag{4}$$

with

$$-\overline{u_i' u_j'} = v_t\left(\frac{\partial u_i}{\partial x_j} + \frac{\partial u_j}{\partial x_i}\right) - \frac{2}{3}k\delta_{ij} \tag{5}$$

Two-equation model for thermal field:

$$\frac{\mathrm{D}T}{\mathrm{D}\tau} = \frac{\partial}{\partial x_j}\left(\alpha\frac{\partial T}{\partial x_j} - \overline{u_j' t}\right) \tag{6}$$

$$\frac{\mathrm{D}\overline{t^2}}{\mathrm{D}\tau} = \frac{\partial}{\partial x_j}\left\{ \left(\alpha + \frac{\alpha_t}{\sigma_h}\right)\frac{\partial \overline{t^2}}{\partial x_j} \right\} - 2\overline{u_j' t}\frac{\partial T}{\partial x_j} - 2\varepsilon_t \tag{7}$$

$$\frac{\mathrm{D}\varepsilon_t}{\mathrm{D}\tau} = \frac{\partial}{\partial x_j}\left\{ \left(\alpha + \frac{\alpha_t}{\sigma_\phi}\right)\frac{\partial \varepsilon_t}{\partial x_j} \right\} - C_{\mathrm{P}1} f_{\mathrm{P}1}\frac{\varepsilon_t}{\overline{t^2}}\overline{u_j' t}\frac{\partial T}{\partial x_j} - C_{\mathrm{P}2}\frac{\varepsilon_t}{k}\overline{u_i' u_j'}\frac{\partial u_i}{\partial x_j} - C_{\mathrm{D}1} f_{\mathrm{D}1}\frac{\varepsilon_t^2}{\overline{t^2}} - C_{\mathrm{D}2} f_{\mathrm{D}2}\frac{\varepsilon\varepsilon_t}{k} \tag{8}$$

with

$$-\overline{u_j' t} = \alpha_t\frac{\partial T}{\partial x_j} \tag{9}$$

where

$$v_t = C_\mu f_\mu k^2/\varepsilon \tag{10}$$

$$\alpha_t = C_\lambda f_\lambda k^2/\varepsilon \tag{11}$$

$$f_\mu = \left\{1 - \exp\left(-\frac{y^*}{14}\right)\right\}^2\left[1 + \frac{5}{R_t^{3/4}}\exp\left\{-\left(\frac{R_t}{200}\right)^2\right\}\right] \tag{12}$$

$$f_\varepsilon = \left\{1 - \exp\left(-\frac{y^*}{3.1}\right)\right\}^2\left[1 - 0.3\exp\left\{-\left(\frac{R_t}{6.5}\right)^2\right\}\right] \tag{13}$$

$$f_\lambda = \left\{\left(\frac{2R}{C_m + R}\right) + 3\frac{(v\varepsilon)^{3/4}}{k^{3/2}}\frac{(2R)^{1/2}}{Pr} f_d\right\} \times \left\{1 - \exp\left(-\frac{y^*}{14}\right)\right\}\left\{1 - \exp\left(-\frac{Pr^{1/2}y^*}{14}\right)\right\} \tag{14}$$

$$f_d = \exp\left\{-\left(\frac{R_t}{200}\right)^2\right\} \tag{15}$$

$$f_{\mathrm{D}1} = \left\{1 - \exp\left(-\frac{y^*}{A_{\mathrm{D}1}}\right)\right\}^2 \tag{16}$$

$$f_{\mathrm{D}2} = \frac{C_{\varepsilon 2} f_2 - 1}{C_{\mathrm{D}2}}\left\{1 - \exp\left(-\frac{y^*}{A_{\mathrm{D}2}}\right)\right\}^2 \tag{17}$$

$$f_2 = 1 - 0.3\exp\left\{-\left(\frac{R_t}{6.5}\right)^2\right\} \tag{18}$$

$$R = (\overline{t^2}/2\varepsilon_t)/(k/\varepsilon) \tag{19}$$

$$R_t = k^2/v\varepsilon \tag{20}$$

$$y^* = \frac{(v\varepsilon)^{1/4} y_n}{v} \tag{21}$$

where the tensor form of the momentum equation represents the u (streamwise) and v (transverse) momentums that are solved, u_i' is the fluctuating velocity component in the i-direction, and p is the pressure. T is the temperature, t is the

Table 1
Model constants appearing in the governing equations

C_μ	σ_k	σ_ε	C_m	$C_{\varepsilon 1}$	$C_{\varepsilon 2}$	C_λ	C_{D1}	C_{D2}	σ_h	σ_ϕ	C_{P1}	C_{P2}	A_{D1}	A_{D2}
0.09	1.4	1.4	0.5	1.5	1.9	0.1	2	0.9	1.6	1.6	1.9	0.6	1	5.7

temperature fluctuation, y_n is the normal distance to the wall surface (the shorter one for the corner situation), $\overline{u_i'u_j'}$ is the Reynolds stress component, and $\overline{u_j't}$ is the turbulent heat flux. The model constants appearing in the governing equations are given in Table 1.

3. Problem statement and code verification

A schematic of the backward-facing step and the computational domain is shown in Fig. 1. The downstream channel's height (H) is maintained as constant of 0.190 m, and the investigated step heights (s) are 0.019, 0.038 and 0.076 m. This provides an expansion ratio (ER $= H/(H-s)$) of 1.11, 1.25 and 1.67, respectively. The length of the computational domain upstream of the step is 0.076 m. The length of the computational domain downstream of the step for ER = 1.11 and 1.25 is 0.760 m, i.e. $-2 \leqslant x/S \leqslant 20$, where S is the channel's reference height (= 0.038 m). The length of the computational domain downstream of the step for ER = 1.67 is 1.140 m, i.e. $-2 \leqslant x/S \leqslant 30$. It was confirmed that a longer computational length does not influence the recirculation flow results. The origin of the coordinate system is located at the bottom corner of the step where the backward-facing step and the downstream stepped wall intersect as shown in Fig. 1.

The physical properties are treated as constants and evaluated for air at the inlet temperature of $T_0 = 20$ °C (i.e. density (ρ) is 1.205 kg/m^3, specific heat (C_p) is 1005 J/(kg °C), molecular dynamic viscosity (μ) is 1.782×10^{-5} kg/(m s), and Prandtl number (Pr) is 0.71). The inlet flow condition (at $x/S = -2$) consists of two developing boundary layers separated by a relatively undisturbed core with a uniform temperature profile ($T_0 = 20$ °C), and these boundary layers have a thickness of $\delta/S = 1.1$. The freestream velocity (u_0) is maintained as constant of 10.86 m/s during these simulations, and the corresponding Reynolds number (Re_0) based on the centerline velocity (u_0) is 28000. The transverse velocity component, v, is taken as zero at the inlet section. Distributions of the inlet turbulent kinetic energy (k) and the turbulence intensity (I) for velocity field are specified based on the experimental data [12,22]. The dissipation rate (ε) for velocity field is obtained from the turbulence intensity and the characteristic length of the inlet channel which is equal to 0.4 δ for the developing boundary layer in the present study. The inlet turbulent kinetic energy ($\overline{t^2}$) for thermal field and its dissipation rate (ε_t) are set as a sufficiently small value of the order of 10^{-12} corresponding to the experimental perturbations at the inlet. The no slip boundary condition is applied at all the wall surfaces. The bottom wall downstream of the step (for $x/S > 0$ and $y/S = 0$) is supplied with a uniform heat flux ($q_w = 270$ W/m^2), while other walls are assumed to be thermally insulated and adiabatic. Boundary conditions at the wall surface for other variables are specified as: $k = \overline{t^2} = 0$, $\varepsilon = 2\nu(\partial\sqrt{k}/\partial n)^2$, and $\varepsilon_t = \alpha(\partial\sqrt{\overline{t^2}}/\partial n)^2$. Fully developed flow and thermal conditions are imposed at the exit section of the calculation domain by equating the streamwise gradients of all quantities except pressure drop at that exit section to zero. Staggered grid arrangement is used and non-uniform grid system is employed in the simulation. The resulting finite volume equations are solved numerically by making use of a line-by-line method combined with alternating direction iteration (ADI) scheme. SIMPLE algorithm is utilized for the computation of pressure correction in the iteration procedure.

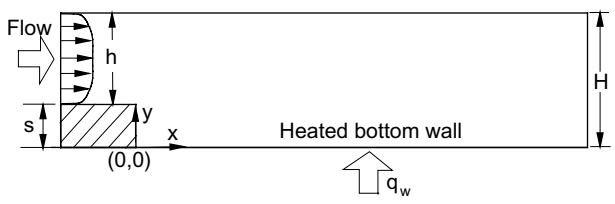

Fig. 1. Schematic of the computational domain.

The present fluid simulation program is an extension over the one that has been used in the earlier work [8,9]. To confirm the accuracy of the present code, the first selected test case is the fully developed thermal field in a two-dimensional turbulent channel flow which was investigated by Kasagi et al. [30] using direct numerical simulation. The bulk Reynolds number ($Re_m = 2u_m\delta/\nu$, where u_m is the averaged velocity) is set to be 4560, and the corresponding Reynolds number based on the friction velocity ($Re_\tau = u_\tau\delta/\nu$) is 150. The grid points are concentrated in the neighborhood of the wall surface to resolve the viscous sublayer accurately and to obtain a grid-independent solution. The calculated mean velocity and temperature profiles are compared with the DNS results, as shown in Fig. 2. The mean velocity and temperature profiles agree very closely with those obtained using direct numerical simulation. The predicted Nusselt number is 15.5 which results in 0.6% discrepancy from the reported DNS data which is 15.4 [30]. An enlarged view for the scale of $y^+ \leqslant 10$ is presented in Fig. 2b. It can be seen that the present simulations give the results in excellent agreement with the DNS data for both velocity and thermal fields.

The other selected test case to validate the turbulent model and the simulation code that are being used in this study is the two-dimensional turbulent flow and heat transfer adjacent to backward-facing step which was experimen-

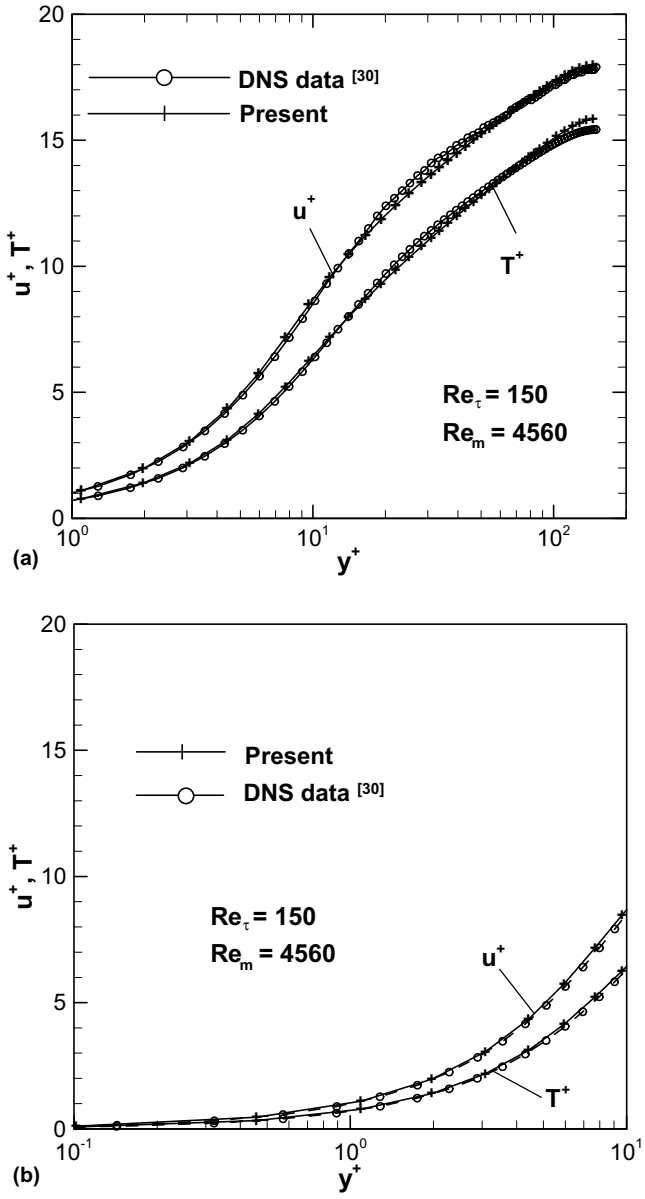

Fig. 2. Comparisons with the DNS data for channel flow and heat transfer.

tally investigated by Adams et al. [12] and Vogel and Eaton [22]. It should be noted that the dimensions and parameters for ER = 1.25 in the present study are identical to those in the experiments. The grid is highly concentrated close to the wall surfaces and near the step corners, in order to ensure the accuracy of the numerical simulation. Grid independence tests were performed using several grid densities and distributions, and the reattachment location on the stepped wall, where the mean streamwise velocity gradient is zero adjacent to the stepped wall, was used as the criteria. A grid of $280(x) \times 116(y)$ downstream of the step was selected for this simulation. Using a denser grid of $360(x) \times 180(y)$ downstream from the step resulted in less than 2.5% difference in the predicted reattachment location. All calculations were performed on the Monarch Empro workstation. The convergence criterion required that the maximum relative mass residual based on the inlet mass be smaller than 10^{-5}. One typical run takes about 60000 iterations in order to achieve the converged solutions. Predicted velocity profiles at several streamwise locations are compared with measurements [12] as shown in Fig. 3 with good agreement between predicted and measured data. This can be seen more clearly with an enlarged view as plotted in Fig. 3b. The predicted reattachment length (x_R/S) is 6.60 and grid resolution ($\Delta x/S$) around the reattachment location is 0.05. The predicted result is in excellent agreement with the measured value of 6.67 [12,22]. Predicted temperature profiles at several streamwise locations are compared with measurements [22] as presented in Fig. 4. The agreement of the simulations with the experiments is very good. Comparison of the computed Stanton number (St) on the heated bottom wall for this test case is made with the available measured data and exhibited in Fig. 5. Very good agreement is obtained for the Stanton number profile inside the recirculation region and near the reattachment region, which justifies the present flow simulation code and provides with confidence for the next simulations. The results which are obtained by using the assumption of constant turbulent Prandtl number ($Pr_t = 0.9$) are also included in the figure. It can be seen that predictions can be greatly improved by using the two-equation turbulence model for the thermal field.

4. Results and discussion

Simulations are performed for turbulent separated and reattached flow and heat transfer adjacent to two-dimensional backward-facing step. Both the velocity and the temperature fields are calculated using two-equation low-Reynolds-number turbulence models [28,29]. Several step heights ($s = 0.019$, 0.038 and 0.076 m) are studied while the freestream velocity (u_0) at the inlet is maintained as constant, in order to investigate effects of step height on the velocity and temperature fields near the reattachment region and adjacent to the step.

Streamlines showing the general flow features for different step heights are presented in Fig. 6. The incoming boundary layer separates at the edge of step because of the sudden change in flow geometry. A primary recirculation region develops adjacent to the step after the boundary separation and shear layer impingement onto the bottom wall. The reattachment length (x_R/S) increases with the increase of the expansion ratio, i.e. step height. They are 3.02, 6.60 and 16.6, respectively, for the step heights of 0.019, 0.038 and 0.076 m. This location also identifies the outer boundary of the primary recirculation region for the two-dimensional flow in this geometry [3,12,22]. The size of the primary recirculation region adjacent to the backward-facing step increases both in length and height with the increase of step height. A small "corner eddy" in the opposite rotation with respect to the primary recirculation flow develops adjacent to bottom corner where the

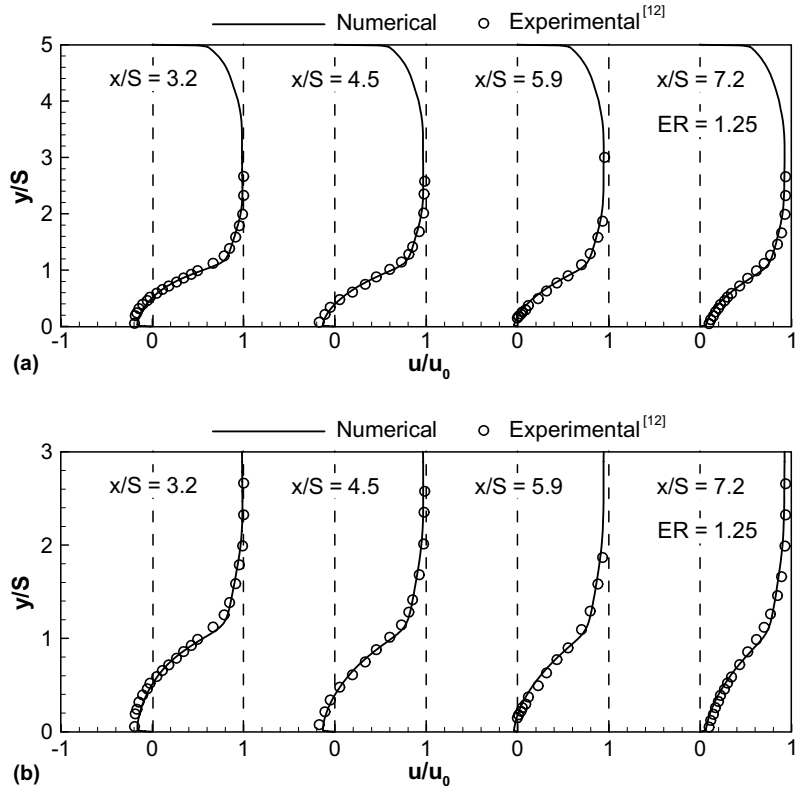

Fig. 3. Comparisons of the mean velocity profiles with the measured data.

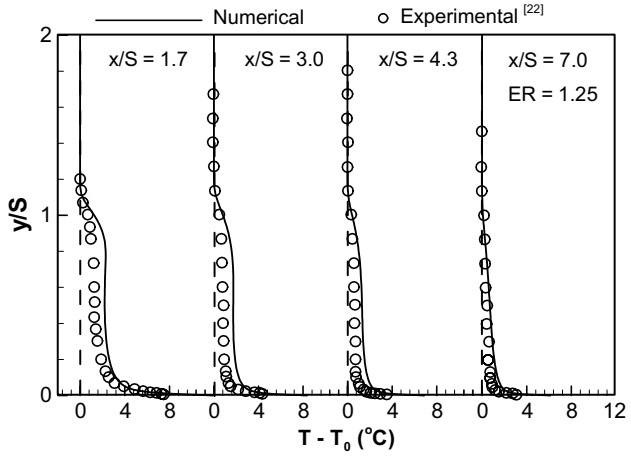

Fig. 4. Comparisons of the mean temperature profiles with the measured data.

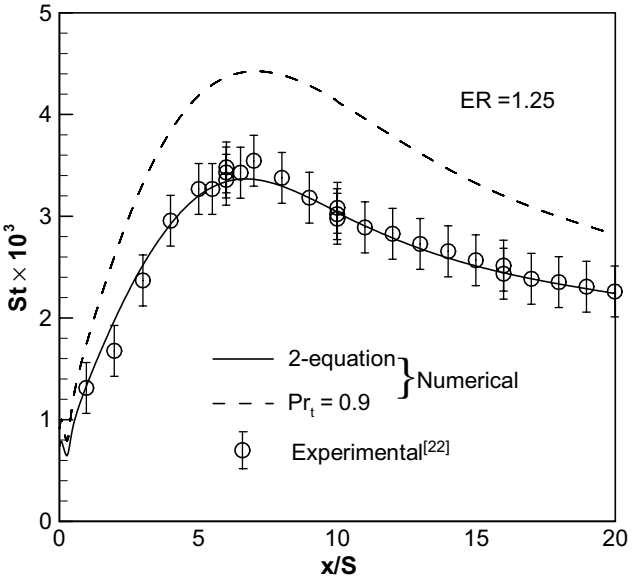

Fig. 5. Comparisons of the Stanton number with the measured data.

step and the bottom wall intersect. Its size also increases with the increase of step height.

Velocity profiles at several streamwise planes are presented in Figs. 7 and 8. Transverse distributions of the mean streamwise velocity component (u) at $x/S = 1, 5, 8$, 10, 15 and 18 are shown in Fig. 7. For the expansion ratio (ER) of 1.11 as shown in Fig. 7a, the reverse flow can be seen on the plane of $x/S = 1$. Flow streams above $y/S > 0.6$ are almost not affected by the recirculation flow that is adjacent to the step, as observed from the velocity profiles at these selected planes except $x/S = 1$. The velocity profile at $x/S = 15$ is almost the same as that at the plane of $x/S = 18$, which represents that flow after the recirculation region recovers downstream of the reattachment point and approaches the fully developed channel flow at this section. For the expansion ratio (ER) of 1.25

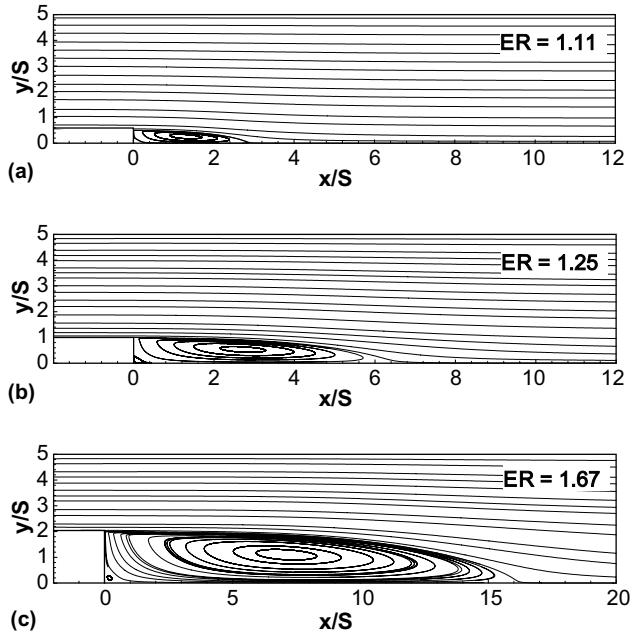

Fig. 6. Streamlines showing the general flow features for different step heights.

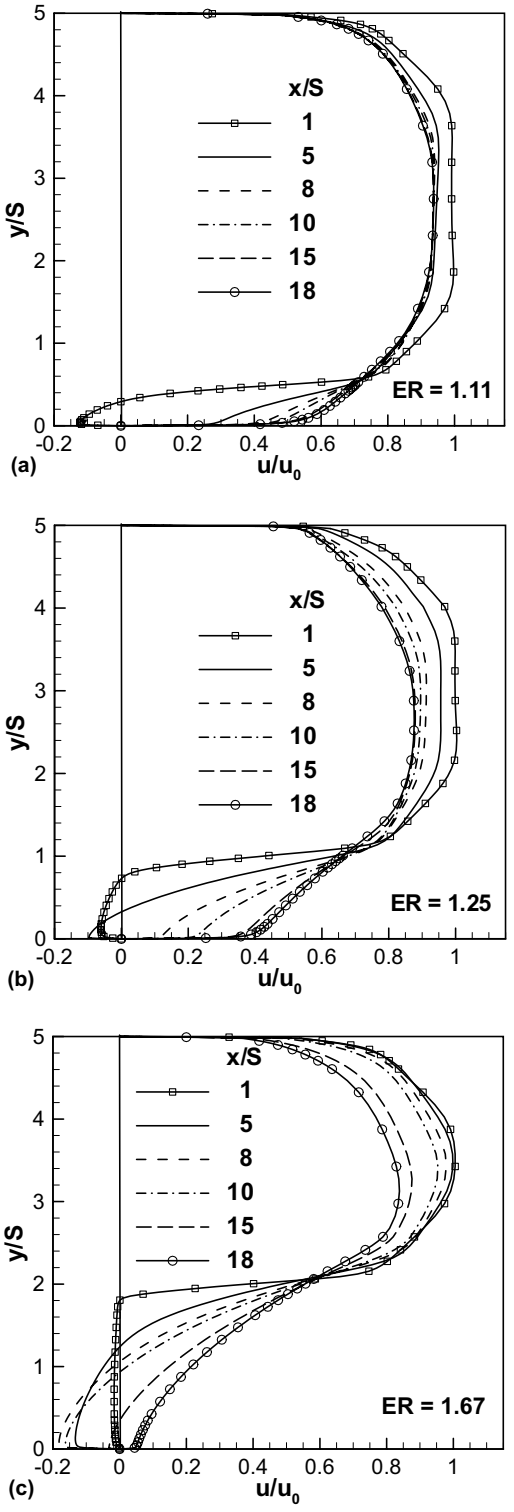

Fig. 7. Distributions of the mean streamwise velocity component (u) at several x-planes.

as shown in Fig. 7b, the reverse flow is observed at the planes of $x/S = 1$ and 5 which are located inside the recirculation region. Effects of the flow recirculation on the upper portion of the velocity profiles are more noticeable for different streamwise locations. This can be seen more clearly for the expansion ratio (ER) of 1.67 as shown in Fig. 7c.

Transverse distributions of the mean velocity component (v) at several x-planes are plotted in Fig. 8. The downwash flow ($v < 0$, flow towards the bottom wall) due to sudden change in flow geometry at step can be observed at these planes above the step height. Magnitude (absolute value) of the maximum v-velocity component ($|v_{\max}|$) at these x-planes increases at the planes upstream of the reattachment location. It then decreases after the reattachment location. For the case of ER = 1.25, the reattachment length is $x_R/S = 6.60$. The $|v_{\max}|$ at $x/S = 5$ is greater than that at $x/S = 1$, then it decreases from $x/S = 5$–8, 10, 15 and 18. This also can be seen from distributions of the gradient of mean transverse velocity component at the stepped wall $\left(\frac{\partial v}{\partial y}|_{\text{wall}}\right)$ as shown in Fig. 9. The peak values of the negative v-velocity component develop at $x/S = 2.91$, 6.28 and 14.9, respectively, for the three expansion ratios. Theses locations are a little shorter than the corresponding reattachment length. The magnitude of negative v-velocity component decreases with the increase of step height. The peak values of the positive v-velocity component (flow away from the bottom wall) also become smaller as the step height increases.

Distributions of the mean temperature field (T) are shown in Fig. 10. The scale of vertical axis is adjusted and set for the best clarity of presentations. The highest temperature develops at the corner and adjacent to the step because of the low convection flow in that region. The maximum temperature difference ($T - T_0$) becomes greater as the step height increases. This also can be seen from Fig. 11 which shows transverse distributions of the mean

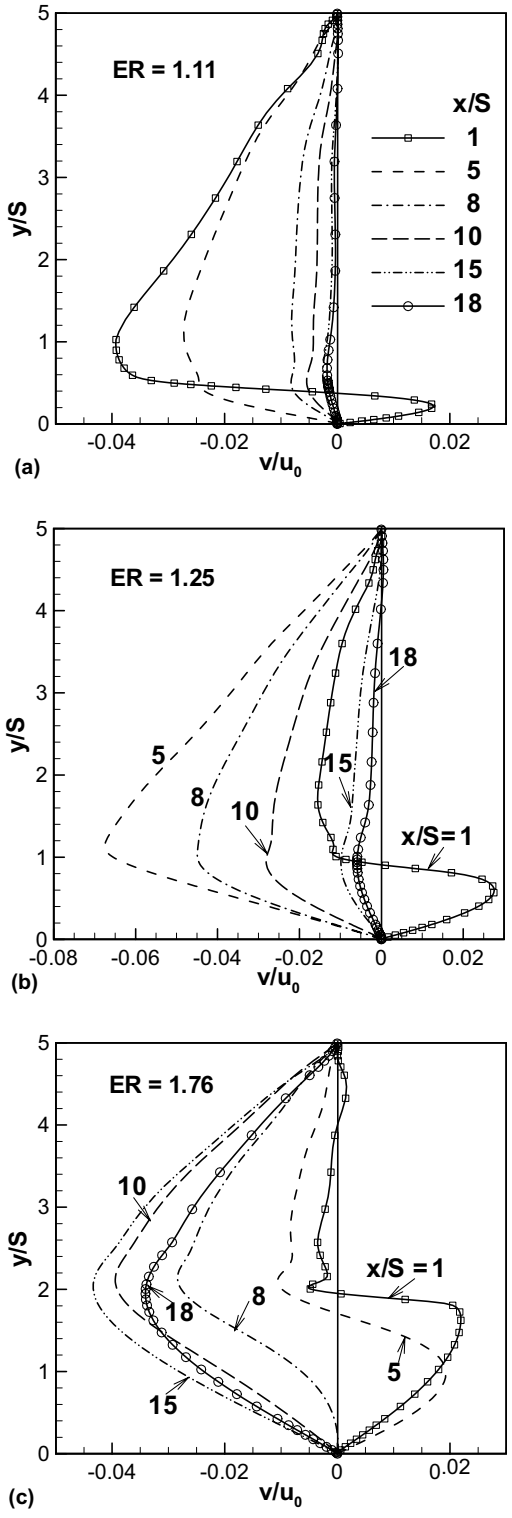

Fig. 8. Distributions of the mean transverse velocity component (v) at several x-planes.

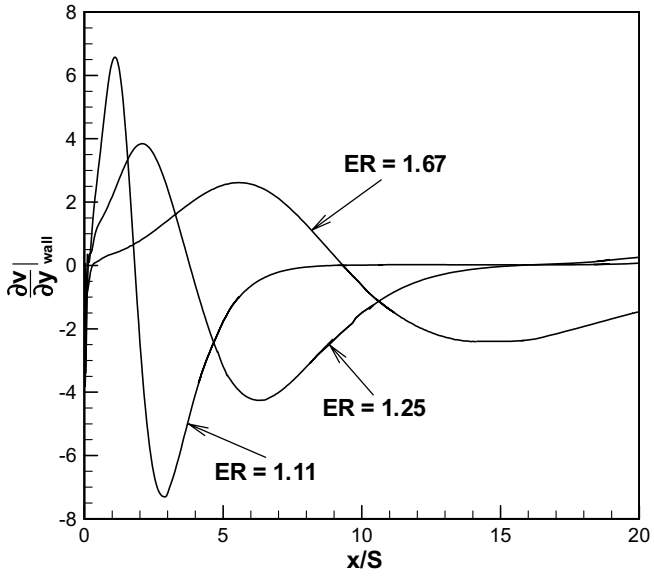

Fig. 9. Distributions of the mean transverse velocity gradient $\left(\frac{\partial v}{\partial y}|_{\text{wall}}\right)$ along the streamwise direction.

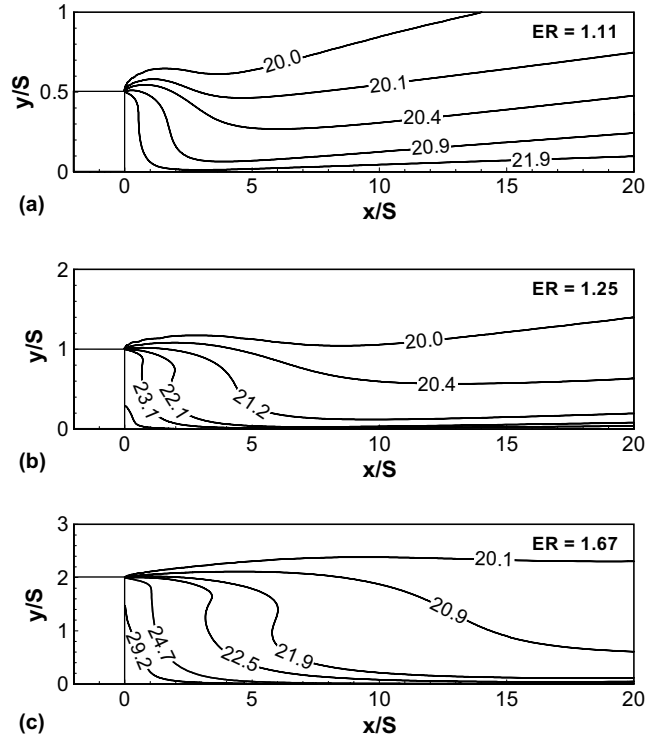

Fig. 10. Distributions of the temperature field for different step heights.

temperature at several streamwise planes. Fig. 11 also shows that at the streamwise locations the temperature does not increase monotonously from the upper wall to the bottom wall as a result of flow recirculation and energy mixing. In Fig. 11b, at $x/S = 1$ for ER = 1.25, the temperature at $y/S = 0.9$ is higher than that at $y/S = 0.5$. This is because the flow at $y/S = 0.9$ and $x/S = 1$ comes from the recirculating flow streams which carry high energy from the region near the reattachment and adjacent to the heated wall. This feature can be seen more clearly with the increase of the step height, as shown in Fig. 10c for ER = 1.67. Distributions of the wall temperature (T_w) are presented in

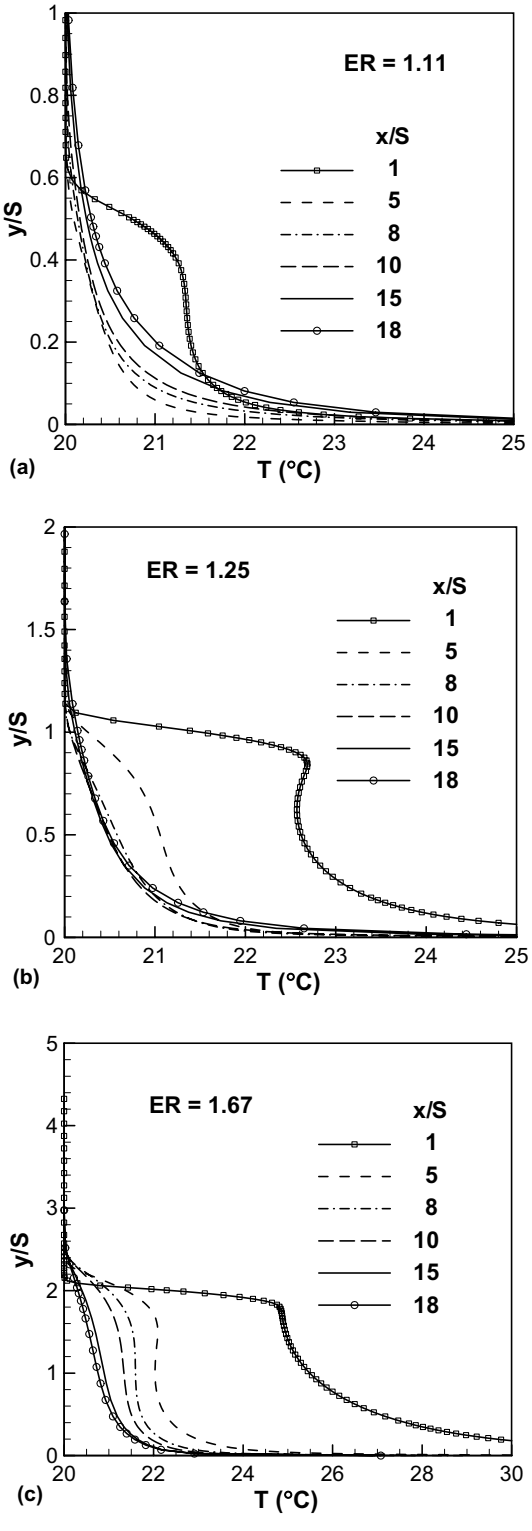

Fig. 11. Distributions of the mean temperature at several x-planes.

Fig. 12. The reattachment location is also included in the figure. They are denoted with the symbol "∇" and the letters A, B, C represent the location for different step heights. The maximum wall temperature appears near the step and its magnitude becomes greater with increase of the step height. Its location, which is a separating point, is associated with the boundary edge of the secondary recirculation region. The wall temperature decreases inside the primary recirculation region and reaches its minimum value near the reattachment region.

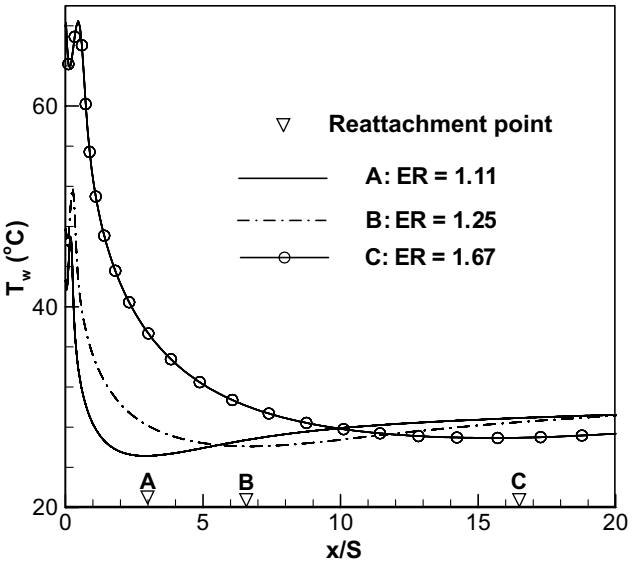

Fig. 12. Distributions of the wall temperature (T_w).

Distributions of the turbulent kinetic energy for velocity field (k) at several x-planes are given in Fig. 13. It should be noted that some of the data points are skipped in the figure for the purpose of clarity. The maximum turbulent kinetic energy develops near the reattachment region and along the separating shear layer. This can be clearly seen from the turbulent kinetic energy profile at the streamwise location near the step such as $x/S = 1$. At this plane, the maximum turbulent kinetic energy is located at approximately the same height as the step edge where the separating shear layer starts. This peak value at the streamwise planes continues to increase inside the recirculation region and reaches its maximum value at the streamwise location around the reattachment location. Increasing the step height causes the magnitude of the maximum turbulent kinetic energy to increase. However, another feature of the turbulent kinetic energy profiles is that at the streamwise plane of $x/S = 1$ below the step height, the turbulent kinetic energy becomes smaller as the step height increases.

Distributions of the friction coefficient (C_f) are shown in Fig. 14. Results for ER = 1.11 and 1.25 are presented only as $x/S \leqslant 20$ and the results downstream of this do not change significantly. The skin friction coefficient and the wall shear stress are minimum (with the zero value) at the reattachment point. Inside the recirculation region, magnitude of the peak friction coefficient does not significantly change with the increase of step height. Downstream of the reattachment point, the skin friction coefficient asymptotically approaches the fully developed channel flow. Its magnitude becomes smaller with the increase of the step height. This is in agreement with the fact that the inlet flowrate (or the bulk Reynolds number) decreases

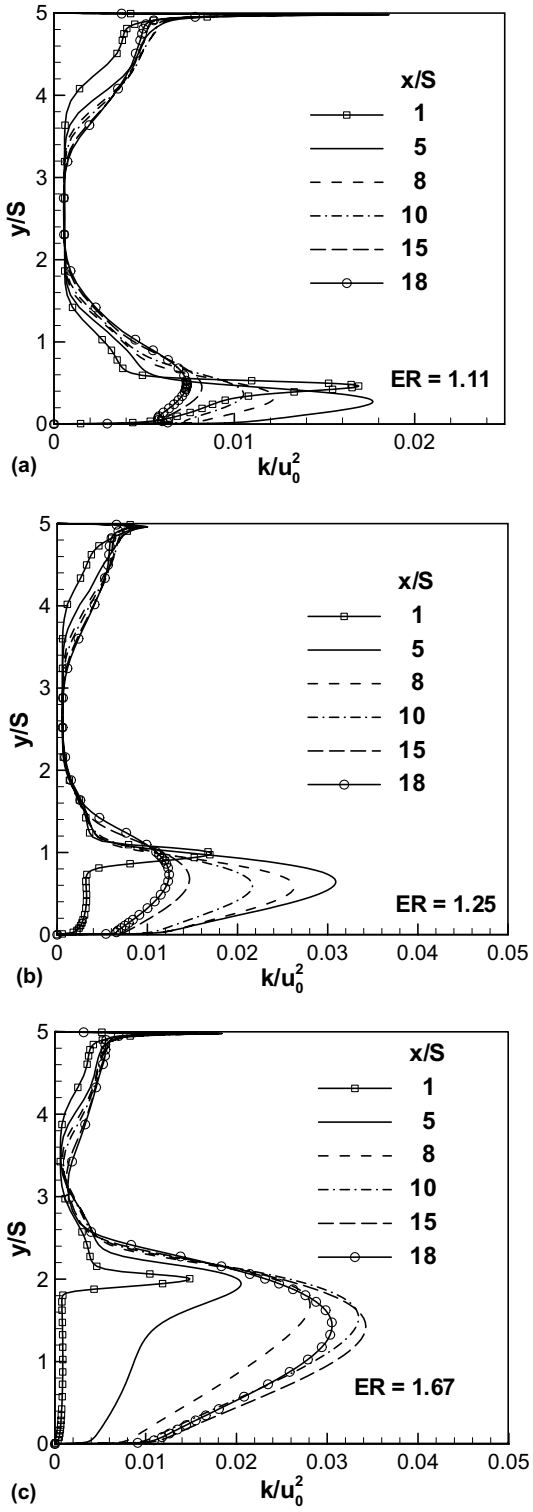

Fig. 13. Distributions of the turbulent kinetic energy for the velocity field at several x-planes.

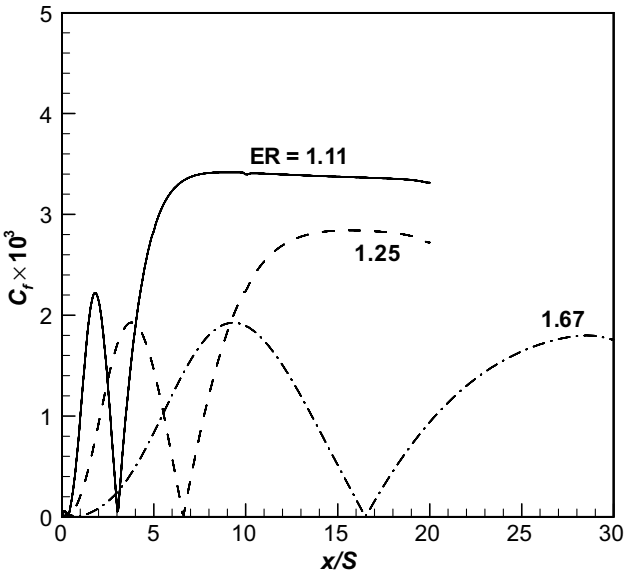

Fig. 14. Distributions of the friction coefficient for different step heights.

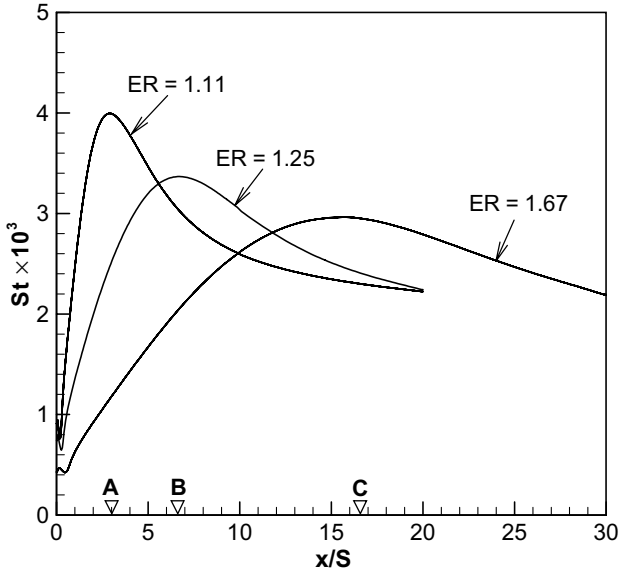

Fig. 15. Distributions of the Stanton number on the stepped wall.

with the increase of step height. The length of flow recovery after reattachment point becomes greater as the step height increases. Fig. 15 represents distributions of the Stanton number (St) at the heated bottom wall. The reattachment locations are also included in the figure with the symbol "∇" in order to show their relative locations. The Stanton number which is inversely in proportion to the wall temperature increases inside the recirculation region and reaches its maximum values around the reattachment location. It decreases downstream of the reattachment point. The maximum Stanton number becomes smaller as the step height increases. Its location moves further downstream with the increase of step height.

5. Conclusions

Numerical simulations are reported for two-dimensional turbulent forced convection flow adjacent to backward-facing step. The primary and secondary recirculation regions

increase as the step height increases. The peak values of the transverse velocity component become smaller as the step height increases. The maximum temperature becomes greater as the step height increases. The bulk temperature increases more rapidly as the step height increases. Increasing the step height causes the magnitude of the maximum turbulent kinetic energy to increase. At the streamwise plane near the step and below the step height, the turbulent kinetic energy becomes smaller as the step height increases. Inside the recirculation region, magnitude of the peak friction coefficient does not significantly change with the increase of step height. Downstream of the reattachment point, the skin friction coefficient asymptotically approaches the fully developed channel flow. Its magnitude becomes smaller with the increase of the step height. The peak Stanton number becomes smaller as the step height increases.

Acknowledgements

This work was in part supported by US Army Research Laboratory under grant DAAD 19-03-2-0007 and by US Department of Energy under grant DE-FG02-03ER46067. The use of computer resources provided by the National Supercomputing Center for Energy and the Environment is gratefully acknowledged.

References

[1] R.L. Simpson, Aspects of turbulent boundary-layer separation, Prog. Aerospace Sci. 32 (5) (1996) 457–521.
[2] J.K. Eaton, J.P. Johnson, A review of research on subsonic turbulent flow reattachment, AIAA J. 19 (9) (1981) 1093–1100.
[3] B.F. Armaly, F. Durst, J.C.F. Pereira, B. Schonung, Experimental and theoretical investigation of backward-facing step flow, J. Fluid Mech. 127 (1983) 473–496.
[4] B.F. Blackwell, D.W. Pepper (Eds.), Benchmark Problems for Heat Transfer Codes, HTD-vol. 222, American Society of Mechanical Engineers, New York, NY, 1992.
[5] B.F. Blackwell, B.F. Armaly (Eds.), Computational Aspects of Heat Transfer—Benchmark Problems, HTD-vol. 258, American Society of Mechanical Engineers, New York, NY, 1993.
[6] D.K. Gartling, A test problem for outflow boundary conditions—flow over a backward-facing step, Int. J. Numer. Meth. Fluids 11 (7) (1990) 953–967.
[7] T. Kondoh, Y. Nagano, T. Tsuji, Computational study of laminar heat-transfer downstream of a backward-facing step, Int. J. Heat Mass Transfer 36 (3) (1993) 577–591.
[8] J.H. Nie, B.F. Armaly, Reverse flow regions in three-dimensional backward-facing step flow, Int. J. Heat Mass Transfer 47 (22) (2004) 4713–4720.
[9] J.H. Nie, B.F. Armaly, Three-dimensional convective flow adjacent to backward-facing step—effects of step height, Int. J. Heat Mass Transfer 45 (12) (2002) 2431–2438.
[10] S. Thangam, D.D. Knight, Effect of stepheight on the separated flow past a backward facing step, Phys. Fluids—A 1 (3) (1989) 604–606.
[11] H. Iwai, K. Nakabe, K. Suzuki, Flow and heat transfer characteristics of backward-facing step laminar flow in a rectangular duct, Int. J. Heat Mass Transfer 43 (3) (2000) 457–471.
[12] E.W. Adams, J.P. Johnston, J.K. Eaton, Experiments on the structure of turbulent reattaching flow, Technical Report MD-43, Thermosciences Division, Department of Mechanical Engineering, Stanford University, 1984.
[13] S. Jovic, D.M. Driver, Backward-facing step measurements at low Reynolds number, $Re_h = 5000$, NASA Technical Memorandum 108807, National Aeronautics and Space Administration, 1994.
[14] J. Kostas, J. Soria, M.S. Chong, Particle image velocimetry measurements of a backward-facing step flow, Exp. Fluids 33 (6) (2002) 838–853.
[15] N. Kasagi, A. Matsunaga, Three-dimensional particle-tracking velocimetry measurement of turbulence statistics and energy budget in a backward-facing step flow, Int. J. Heat Fluid Flow 16 (6) (1995) 477–485.
[16] O.O. Badran, H.H. Bruun, Comparison of flying-hot-wire and stationary-hot-wire measurements of flow over a backward-facing step, ASME J. Fluids Eng. 121 (2) (1999) 441–445.
[17] H. Le, P. Moin, J. Kim, Direct numerical simulation of turbulent flow over a backward-facing step, J. Fluid Mech. 330 (1997) 349–374.
[18] S. Tangam, C.G. Speziale, Turbulent flow past a backward-facing step: a critical evaluation of two-equation models, AIAA J. 30 (5) (1992) 1314–1320.
[19] H.Q. Zhang, C.K. Chan, K.S. Lau, Numerical simulation of sudden-expansion particle-laden flows using an improved stochastic flow model, Numer. Heat Transfer: Part A—Appl. 40 (1) (2001) 89–102.
[20] O. Labbe, P. Sagaut, E. Montreuil, Large-eddy simulation of heat transfer over a backward-facing step, Numer. Heat Transfer: Part A—Appl. 42 (1–2) (2002) 73–90.
[21] R.V.R. Avancha, R.H. Pletcher, Large eddy simulation of the turbulent flow past a backward-facing step with heat transfer and property variations, Int. J. Heat Fluid Flow 23 (5) (2002) 601–614.
[22] J.C. Vogel, J.K. Eaton, Combined heat transfer and fluid dynamic measurements downstream of a backward-facing step, ASME J. Heat Transfer 107 (4) (1985) 922–929.
[23] G.H. Rhee, H.J. Sung, Enhancement of heat transfer in turbulent separated and reattaching flow by local forcing, Numer. Heat Transfer: Part A—Appl. 37 (2) (2000) 733–753.
[24] K. Hanjalic, Will RANS survive LES? A view of perspectives, ASME J. Fluids Eng. 127 (5) (2005) 831–839.
[25] B.E. Launder, On the computation of convective heat-transfer in complex turbulent flows, ASME J. Heat Transfer 110 (4B) (1988) 1112–1128.
[26] W.P. Jones, B.E. Launder, The prediction of laminarization with a two-equation model of turbulence, Int. J. Heat Mass Transfer 15 (2) (1972) 301–314.
[27] C.K.G. Lam, K. Bremhorst, A modified form of the k–ε model for predicting wall turbulence, ASME J. Fluids Eng. 103 (3) (1981) 456–460.
[28] K. Abe, T. Kondoh, Y. Nagano, A new turbulence model for predicting fluid flow and heat transfer in separating and reattaching flows—I. Flow field calculations, Int. J. Heat Mass Transfer 37 (1) (1994) 139–151.
[29] K. Abe, T. Kondoh, Y. Nagano, A new turbulence model for predicting fluid flow and heat transfer in separating and reattaching flows—II. Thermal field calculations, Int. J. Heat Mass Transfer 38 (8) (1995) 1467–1481.
[30] N. Kasagi, Y. Tomita, A. Kuroda, Direct numerical simulation of passive scalar field in a turbulent channel flow, ASME J. Heat Transfer 114 (3) (1992) 598–606.